Statistical Modeling of Single-Photon Avalanche Diode Receivers for Optical Wireless Communications

Statistical Modeling of Single-Photon Avalanche Diode Receivers for Optical Wireless Communications

Elham Sarbazi, *Student Member, IEEE,* Majid Safari, *Member, IEEE,* and Harald Haas, *Fellow Member, IEEE*

***Abstract*—In this paper, a comprehensive analytical approach is presented for modeling the counting statistics of active quenching and passive quenching single photon avalanche diode (SPAD) detectors. It is shown that, unlike ideal photon counting receiver for which the detection process is described by a Poisson arrival process, photon counts in practical SPAD receivers do not follow a Poisson distribution and are highly affected by the dead time caused by the quenching circuit. Using the concepts of renewal theory, the exact expressions for the probability distribution and moments (mean and variance) of photocounts in the presence of dead time are derived for both active quenching and passive quenching SPADs. The derived probability distributions are validated through Monte Carlo simulations and it is demonstrated that the moments match with the existing empirical models for the moments of SPAD photocounts. Furthermore, an optical communication system with on-off keying (OOK) and binary pulse position modulation (BPPM) is considered and the bit error performance of the system for different dead time values and background count levels is evaluated.**

***Index Terms*—Single photon avalanche diode (SPAD), optical wireless communications, photon counting, dead time, active quenching, passive quenching, on-off keying (OOK), binary pulse position modulation (BPPM).**

I. Introduction

In recent years, there has been a growing interest in optical wireless communications (OWC) as a promising complementary solution to radio frequency (RF) technologies [1]. OWC systems primarily use positive-intrinsic-negative (PIN) diodes and avalanche photodiodes (APDs) as optical receivers. PIN diodes have simple structure and are relatively inexpensive. The main disadvantage of PIN diodes is their low gain. When operating at extremely low signal levels, their thermal noise can be more significant than the signal. Compared to PIN diodes, APDs are more complicated and expensive. They outperform PIN diodes with respect to sensitivity, as their internal gain reduces the thermal noise effect. However, the random multiplication process introduces additional gain-dependent excess noise, and this limits the maximum achievable gain of an APD. Therefore, high gain low noise transimpedance amplifiers (TIAs) are usually required for detection of relatively weak optical signals [2].

In photon-starving applications and long distance transmissions, the optical signal can be received at levels below the sensitivity of these conventional optical receivers and get lost in the thermal noise. Single photon avalanche diodes (SPADs) appear to be a more proper choice in such applications. SPADs provide very large internal gain, thereby easily overcoming thermal noise and enabling the detection of individual photons without the need for TIAs. Thanks to their high single-photon sensitivity and high gain, SPADs have enabled rapid progress in many applications [3]–[5]. These receivers are able to closely approach quantum-limited sensitivity in the detection of weak optical signals and have drawn particular attention in OWC [6]–[12].

SPADs are semiconductor devices with p-n junctions and operate based on a simple principle: if the reverse bias voltage of the p-n junction is raised slightly above the breakdown threshold voltage, a very high electric field is produced, and a single electron-hole pair, can trigger a strong avalanche, leading to a large internal gain and a measurable current. This current rises rapidly and continues until the avalanche is quenched by lowering the bias voltage down to or below breakdown threshold [13], [14]. To detect a subsequent photon, the bias voltage must be raised again above breakdown level. Reducing the bias voltage below the threshold and restoring the SPAD to the operative level, is accomplished by *quenching circuit*. The quenching process introduces a finite recovery time, known as *dead time*, during which the device does not respond to another incident photon [15].

There are two principal quenching modes: *passive quenching* (PQ) and *active quenching* (AQ). In general, AQ circuits offer shorter dead times and higher count rates compared with PQ circuits, but are more complex, more expensive to fabricate and larger in size [16]. The photon counting process of PQ SPADs is similar to *paralyzable* detectors where any photon arriving during dead time is not counted, but extends the dead time period. In AQ SPADs, similar to *nonparalyzable* detectors, the dead time is constant, and any photon arriving during dead time is neither counted nor it extends the dead time duration [16].

SPADs are still a relatively immature technology whose performance is degraded by the unavoidable dead time. The dead time is a limiting factor for the achievable data rate in OWC systems. Because of demands for higher data rates, several studies has been recently dedicated to reducing the effect of dead time by employing arrays of SPADs [17]–[20]. From a communication theory point of view, it is of great importance to investigate the effect of dead time on the performance of an SPAD-based OWC system. For this purpose, the statistical dead time-affected photon counting

The authors are with the Li-Fi Research and Development Centre, Institute for Digital Communications, School of Engineering, The University of Edinburgh, Edinburgh EH9 3JL, UK (e-mail: e.sarbazi@ed.ac.uk; majid.safari@ed.ac.uk; h.haas@ed.ac.uk).

behavior of SPAD receivers needs to be precisely modeled.

Previous Works: In [21], the paralyzable and nonparalyzable count rate models are introduced which are the most well-known models for estimating the count rate of a single-photon detector. These two models have also been adopted for SPAD detectors to predict the approximate count rate [22]. The count rate is a useful metric for assessing how fast the detector can detect incoming photons. However, it does not provide a complete description of the detected and lost photons, required for error performance evaluation of communication systems. In [6], a SPAD-based VLC system with OOK modulation is proposed to address the problem of continuous downhole monitoring in the oil and gas industry. In this article, a SPAD array is considered, and the counting losses due to SPAD's dead time have not been taken into account. In [7] and [8], a SPAD-based optical orthogonal frequency division multiplexing (OFDM) system is presented and the nonlinear distortion due to the saturation of SPAD receiver, as well as the bit error ratio performance of both DC-biased optical OFDM and asymmetrically clipped optical OFDM are investigated. Authors in [7] and [8], have assumed Poisson statistics for the distribution of SPAD photocounts, which is not an accurate approximation in the presence of dead time. In [23], the method of contour integration is used for deriving the photon counting distribution of a single-photon detector with paralyzable dead time. In [24], using the concepts of Poisson point processes, the effect of a nonparalyzable dead time is studied. In [25], a practical photon counting receiver in optical scattering communication with finite sampling rate, paralyzable dead time, and electrical noise is characterized where it is shown that the dead time effect leads to sub-Poisson distribution for the number of recorded pulses. The approximate photocount distribution derived in [25], is only applicable if the photon rate is sufficiently low. In [26], we studied the statistical behavior of an AQ SPAD receiver and investigated the effect of nonparalyzable dead time on the bit error performance of an optical system. We extended our approach in [27] and an array of AQ SPADs was characterized for OWC applications. We also studied the information transfer rate of an AQ SPAD in [28] where the AQ SPAD receiver was modeled as a discrete memoryless channel, and the information transfer rate was studied using an information theoretic approach.

Our Contribution: In this study, we establish a mathematical framework and precisely model the photon counting behavior of SPAD receivers. We apply the concepts of renewal theory to develop exact expression for the probability distribution of photon counts in the presence of a general type of dead time, and then provide the exact probability distribution, mean and variance of AQ and PQ SPAD photocounts. Moreover, we study the bit error performance of a SPAD-based optical link. This study shows that the counting process of a SPAD receiver in the presence of dead time cannot be accurately approximated by a Poisson distribution. To the best of our knowledge, there exists limited, if not any analytical work to find the exact photocount distribution of SPAD photocounts, considering the impact of dead time. Although the main focus of this article is on SPAD detectors, but the approach can be applied to a variety of single-photon detectors with similar photon counting behavior.

The rest of this paper is organized as follows. In Section II, the concepts of renewal theory are applied for modeling the exact dead time-modified photocount distribution of a detector with a general type of dead time. The exact photocount distribution of AQ and PQ SPAD receivers are then derived in Section III using the results obtained in Section II, and Monte Carlo methods are employed to verify the validity of the analytical models. The system model of a SPAD-based optical system is described in Section IV, and in Section V, the numerical and analytical results are compared and discussions on the bit error performance of the system are provided. Finally, concluding remarks are given in Section VI.

II. Description of the Theoretical Framework

In this section, first the concepts of "product density functions" and "renewal processes" are introduced. These tools are then applied for modeling the dead time-modified photocount distribution of SPAD receivers based on a general approach that can be applied to both AQ and PQ SPADs.

A. Product Density Functions

Consider a stochastic point process N corresponding to events occurring at times $\{t_i\}$, $i = 0, 1, \ldots$. Let $N(t)$ represent the stochastic variable denoting the number of events in the time interval $(0, t)$. Then $dN(t)$ denotes the number of events in the small interval $(t, t + dt]$. A function $f_1(t)dt$ is defined such that [29]:

$$f_1(t)dt = E[dN(t)] \,, \tag{1}$$

where $E[dN(t)]$ represents the average number of events in interval $(t, t + dt]$. Accordingly, the product of two stochastic variables $dN(t_1)$ and $dN(t_2)$ is defined as [29]:

$$f_2(t_1, t_2)dt_1dt_2 = E[dN(t_1)dN(t_2)] \,, \tag{2}$$

which is also equal to the joint probability that an event occurs in $(t_1, t_1 + dt_1]$ and another event occurs in $(t_2, t_2 + dt_2]$. The function f_2 is called a product density of order 2. Similarly, the product density function of order k, $f_k(t_1, t_2, \ldots, t_k)$, is defined as [29]:

$$f_k(t_1, t_2, \ldots, t_k)dt_1dt_2 \ldots dt_k = E[dN(t_1) \ldots dN(t_k)] \,, \tag{3}$$

where $f_k(t_1, t_2, \ldots, t_k)dt_1dt_2 \ldots dt_k$ represents the probability that an event occurs in the interval between t_1 and $t_1 + dt_1$, one event between t_2 and $t_2 + dt_2$, ..., and one between t_k and $t_k + dt_k$.

Provided that $t_1, t_2, \ldots, t_k$ are ordered ($t_1 < t_2 < \cdots < t_k$) and the general class of Poisson processes is considered, the following equation holds between the product density of order k and the product densities of order one [29]:

$$f_k(t_1, t_2, \ldots, t_k) = f_1(t_1)f_1(t_2 - t_1) \ldots f_1(t_k - t_{k-1}) \,. \tag{4}$$

We shall now apply the above tools to the problem of modeling the exact counting distribution of a SPAD receiver impaired by dead time. The aim is to determine $p(k, t)$, the probability that k photons have been detected during time

$$\left.\frac{\partial^k G(z,t)}{\partial z^k}\right|_{z=1} = k! \int_0^t dt_k \int_0^{t_k} dt_{k-1} \ \ldots \int_0^{t_3} dt_2 \int_0^{t_2} f_1(t_1) f_1(t_2 - t_1) \ldots f_1(t_k - t_{k-1})\, dt_1 \ , \tag{7}$$

interval $(0, t)$. It is clear that what happens between t and $t + dt$ is not only dependent on the fact that k photons have been detected in time interval $(0, t)$, but also upon the detection time of last photon, due to dead time. Hence, the usual method of expressing $p(k, t+dt)$ in terms of $p(k, t)$ is mathematically involved. We first determine $G(z, t)$, the generating function (G.F.) corresponding to $p(k, t)$, which is given by:

$$G(z,t) = \sum_{k=0}^{\infty} p(k,t) z^k. \tag{5}$$

The following property holds for $G(z, t)$ and the product density of order k [29]:

$$\left.\frac{\partial^k G(z,t)}{\partial z^k}\right|_{z=1} = \int_0^t \int_0^t \ldots \int_0^t f_k(t_1, t_2, \ldots, t_k)\, dt_1 dt_2 \ldots dt_k \ . \tag{6}$$

Note that f_k is symmetrical in t_1, t_2, ..., t_k, and (6) can be written as (7) at the top of this page. The following equation is then deduced from (7):

$$\left.\frac{\partial G(z,t)}{\partial z}\right|_{z=1} = \int_0^t f_1(t_1)\, dt_1 \tag{8}$$

Now, let the Laplace transform (L.T.) of the function $f_1(t)$ with respect to the variable t be $F_1(s) = \int_0^\infty f_1(t)\, e^{-st} dt$. Taking the L.T. of (8) gives:

$$g(z,s) = \frac{1}{s} \times \frac{1}{1 - (z-1)F_1(s)} \ , \tag{9}$$

where $g(z, s)$ is the L.T. of the function $G(z, t)$. Let also define $P(k, s)$ as the L.T. of the function $p(k, t)$. The following diagram summarizes how the four functions $p(k, t)$, $P(k, s)$, $G(z, t)$, and $g(z, s)$ are connected:

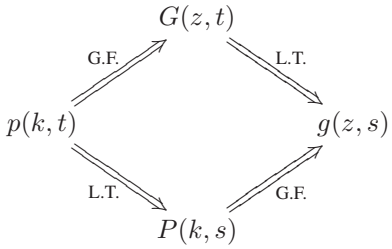

Since $g(z, s)$ is the G.F. of $P(k, s)$, according to (9), $P(k, s)$ can be obtained as [30]:

$$P(k,s) = \frac{1}{s} \times \frac{[F_1(s)]^k}{[1 + F_1(s)]^{k+1}} \ . \tag{10}$$

From this, it can be concluded that if $f_1(t)$ or $F_1(s)$ is known for the point process associated with the SPAD's photon counting process, $P(k, s)$, and hence, $p(k, t)$ can be obtained.

B. Renewal Processes

By definition, a counting process $\omega = \{N(t) : t \geq 0\}$ with the occurrence time sequence of $\{t_i\}$, is called a renewal process if the inter-occurrence times $w_1 = t_1 - t_0$, $w_2 = t_2 - t_1$, ... are independently and identically distributed random variables. In the case of a Poisson point process, the inter-occurrence times are independently and identically distributed exponential random variables [29]. In this work, assuming a Poisson arrival process for incoming photons, the photon counts form a renewal counting process with:

$$p(k,t) = \Pr\{N(t) = k\} \ . \tag{11}$$

For renewal processes, the usual method for obtaining $p(k, t)$ is through renewal integral equations in which $p(k, t)$ is expressed in terms of $p(k-1, t)$. This requires the use of product density functions as introduced earlier. First, please note that the equation in (4) between the product densities of order 1 and k implies that given an event at $t = 0$, the probability that an event occurs between t and $t + dt$ is determined by $f_1(t)dt$ and is independent of what happened before $t = 0$.

Consider a SPAD detector with dead time τ (whether paralyzable or nonparalyzable or a combination of both). For simplicity, normalized photon arrival rate is assumed throughout the derivations. Given a photon registered at $t = 0$, if the *next* photon arrives in the time period of $(0, \tau)$ it is not detected, but if it arrives after the dead time of the photon occurring at $t = 0$, it is counted. The probability that the *next* photon arrives between t' and $t' + dt'$, given that the first photon is registered at $t = 0$, can be expressed by the function $(-\partial\phi(t')/\partial t')dt'$ where $\phi(t)$ represents the probability that no photon arrives between 0 and t, given that a photon arrived at $t = 0$ [29]. The integral equation for this renewal process can be written as:

$$p(k,t) = \int_0^t p(k-1, t-t')(-\frac{\partial\phi(t')}{\partial t'})dt' + \delta(k)\phi(t) \ , \tag{12}$$

where $\delta(k) = 1$ for $k = 0$ and 0 otherwise. In the above renewal equation, the first term in the right-hand side, accounts for the case where the next photon arrives between t' and $t' + dt'$. This photon is not detected if $0 < t' \leq \tau$. The second term represents the case where no photon arrives during time interval $(0, t)$. The following equation holds for the G.F. corresponding to $p(k, t)$:

$$G(z,t) = \int_0^t z\, G(z, t-t')(-\frac{\partial\phi(t')}{\partial t'})dt' + \phi(t) \ . \tag{13}$$

Taking the L.T. of the above equation with respect to the variable t gives:

$$g(z,s) = \frac{\Phi(s)}{1 + z(s\,\Phi(s) - 1)} \ , \tag{14}$$

$$p(k,t) = \sum_{r=0}^{K_1} (-1)^r \binom{k+r-1}{r} \frac{(t-k\tau_1 - r\tau_2)^{k+r}}{(k+r)!} e^{-(k+r)\tau_2} - \sum_{r=0}^{K_2} (-1)^r \binom{k+r}{r} \frac{(t-(k+1)\tau_1 - r\tau_2)^{k+r+1}}{(k+r+1)!} e^{-(k+r+1)\tau_2}, \tag{16}$$

where $\Phi(s)$, is the L.T. of the function $\phi(t)$. Since $g(z,s)$ is also the G.F. of $P(k,s)$, according to (14), $P(k,s)$ is given by [30]:

$$P(k,s) = \Phi(s)(1 - s\,\Phi(s))^k \ . \tag{15}$$

Thus, if $\phi(t)$ (and hence, $\Phi(s)$) is known for SPAD's photon counting renewal process, $p(k,t)$ can be obtained by finding the inverse L.T. of the above equation.

C. A Solution for SPAD Receivers with Dead time

The above results can now be applied to derive the probability distribution function $p(k,t)$ of the number of detected photons, k, in a time interval of $(0,t)$ in the presence of detector dead time. Here, a general approach is proposed which provides the dead time-modified photocount distribution of any photon counting detector. Note that AQ and PQ SPADs are special cases and will be addressed later in Section III.

Suppose that detected and lost photons are followed by two different dead times, τ_1 and τ_2, respectively. Assuming different dead time values for detected and lost photons, helps to clearly reflect distinct effects of paralyzable and nonparalyzable dead times on the total renewal process. For such a detector, we have the following results.

Theorem 1: For a general photon counting detector with dead times τ_1 and τ_2, the probability distribution function, $p(k,t)$, of the number of detected photons, k, in a time interval $(0,t)$ is given by (16) at the top of this page where K_1 and K_2 are integers such that:

$$\frac{t-k\tau_1}{\tau_2} - 1 < K_1 < \frac{t-k\tau_1}{\tau_2}$$
$$\frac{t-(k+1)\tau_1}{\tau_2} - 1 < K_2 < \frac{t-(k+1)\tau_1}{\tau_2}.$$

Proof: Assume that $\tau_1 > \tau_2$. The probability $\phi(t)$ that no photon is detected up to time t, given that a photon is registered at $t = 0$, is:

$$\phi(t) = [\mathbf{1}(t) - \mathbf{1}(t-(\tau_1-\tau_2))] + \phi^{\mathrm{p}}(t-(\tau_1-\tau_2))\mathbf{1}(t-(\tau_1-\tau_2)) \ , \tag{17}$$

where $\mathbf{1}(t)$ is the unit step function, and is equal to 1 if $t \geq 0$, and 0, otherwise. In the above equation, the total probability of not detecting any photons is obtained as follows: The first term in the right-hand side of (17) expresses the condition that no photon is detected for $t < \tau_1 - \tau_2$. If any photon arrives during time interval of $(0, \tau_1 - \tau_2)$, it is clearly lost and is followed by a dead time of length τ_2, and this dead time won't extend beyond the dead time caused by the registered photon at $t = 0$, i.e. τ_1. Thus, $\phi(t) = 1$ for $t < \tau_1 - \tau_2$. If any photon arrives after $\tau_1 - \tau_2$, the dead time will be extended beyond τ_1. It is then valid to assume that the detector is in paralyzable mode, where $\phi^{\mathrm{p}}(t-(\tau_1-\tau_2))$ represents the probability that no photon is registered in time $t-(\tau_1-\tau_2)$. Applying L.T. to (17) gives:

$$\Phi(s) = \frac{1}{s}(1 - e^{-s(\tau_1-\tau_2)}) + e^{-s(\tau_1-\tau_2)}\Phi^{\mathrm{p}}(s) \ . \tag{18}$$

In order to obtain $\Phi^{\mathrm{p}}(s)$ and then $\Phi(s)$, the product density of the first order for the paralyzable mode is easily calculated as:

$$f_1{}^{\mathrm{p}}(t)dt = \mathbf{1}(t-\tau_2)e^{-\tau_2}dt \ . \tag{19}$$

The above expression results from arguing that a photon is detected if it arrives after the dead time of the photon at $t = 0$ is finished ($t > \tau_2$) and it is also not preceded by any photon arrival event in time interval $(0, \tau_2)$. Thus:

$$F_1{}^{\mathrm{p}}(s) = \frac{1}{s}e^{-(s+1)\tau_2} \ . \tag{20}$$

$F_1{}^{\mathrm{p}}(s)$ and $\Phi^{\mathrm{p}}(s)$ are related through (9) and (14):

$$\Phi^{\mathrm{p}}(s) = \frac{1}{s} \times \frac{1}{1 + F_1{}^{\mathrm{p}}(s)} \ . \tag{21}$$

Therefore, (18), (20) and (21) result in:

$$F_1(s) = \frac{1}{s\ e^{s\tau_1+\tau_2} + e^{s(\tau_1-\tau_2)} - 1} \ . \tag{22}$$

The same result is obtained for $\tau_1 < \tau_2$ following exactly the same arguments. According to (10), for general values of τ_1 and τ_2, the expression in (23) at the top of next page is obtained for $P(k,s)$. Applying the inverse L.T. then leads to (24). Using the following equality for $t > 0$:

$$\frac{1}{2\pi i}\int_{\alpha-i\infty}^{\alpha+i\infty} \frac{e^{st}}{s^k}\, ds = \frac{t^{k-1}}{(k-1)!} \ ,$$

the final expression in (16) for $p(k,t)$ is obtained. This completes the proof for Theorem 1. ∎

When $\tau_1 \neq 0$ and $\tau_2 \neq 0$, $p(k,t)$ is given by a finite series. Particular cases include:

- With $\tau_2 = 0$, the photocount distribution for an AQ SPAD is obtained.
- With $\tau_1 = \tau_2$, the photocount distribution for a PQ SPAD is obtained.
- With $\tau_1 = \tau_2 = 0$, the Poisson distribution for an ideal detector is obtained.

Note that the dead time of detected and lost photons are not the same in general, e.g. for an AQ SPAD. In the next section, AQ and PQ SPADs are studied in detail.

$$P(k,s)=\frac{1}{s}\left[\left(e^{s\tau_1+\tau_2}+e^{s(\tau_1-\tau_2)}\right)^{-k}-\left(e^{s\tau_1+\tau_2}+e^{s(\tau_1-\tau_2)}\right)^{-(k+1)}\right] \tag{23}$$

$$\begin{aligned}p(k,t)&=\frac{1}{2\pi i}\int_{\alpha-i\infty}^{\alpha+i\infty}\left[\frac{1}{s}\left(e^{s\tau_1+\tau_2}+e^{s(\tau_1-\tau_2)}\right)^{-k}-\frac{1}{s}\left(e^{s\tau_1+\tau_2}+e^{s(\tau_1-\tau_2)}\right)^{-(k+1)}\right]e^{st}ds\\&=\frac{1}{2\pi i}\int_{\alpha-i\infty}^{\alpha+i\infty}\sum_{r=0}^{\infty}\left[e^{-(k+r)\tau_2}(-1)^r\binom{k+r-1}{r}\frac{e^{s(t-k\tau_1-r\tau_2)}}{s^{k+r+1}}\right]ds\\&\quad-\frac{1}{2\pi i}\int_{\alpha-i\infty}^{\alpha+i\infty}\sum_{r=0}^{\infty}\left[e^{-(k+r+1)\tau_2}(-1)^r\binom{k+r}{r}\frac{e^{s(t-(k+1)\tau_1-r\tau_2)}}{s^{k+r+2}}\right]ds\end{aligned} \tag{24}$$

III. SPAD's Counting Statistics

In the absence of dead time, photon detection events of a SPAD receiver are modeled as a Poisson process and the probability of counting k photons during a time period of $(0,T_{\rm b})$ is given by [1]:

$$p_0(k)=\frac{(\lambda T_{\rm b})^k e^{-\lambda T_{\rm b}}}{k!}\,, \tag{25}$$

where the constant λ is the average photon arrival rate (in photons/s), hence, $\lambda T_{\rm b}$ is the average number of photons arriving at the SPAD during the observation time of $T_{\rm b}$ seconds. The photon arrival rate λ is related to the power of the optical signal by [1]:

$$\lambda=\frac{\eta_{\rm QE}P_{\rm r}}{h\nu}\,, \tag{26}$$

where $\eta_{\rm QE}$ is the quantum efficiency of the SPAD; $P_{\rm r}$ denotes the power of the incident optical signal; h is the Planck's constant; and ν represents the frequency of the optical signal.

In the presence of dead time, however, the photon counts no longer follow a Poisson distribution. In this section, the results of previous section are applied to study the counting statistics of AQ and PQ SPAD receivers. Throughout this work, it is assumed that the sampling rate is very high compared to dead time, so that the counting losses arising from finite sampling rates are negligible. It is also assumed that the SPAD uses the rising edge of a pulse as an event to count. Therefore, the total number of counted photons during the counting interval of $(0,T_{\rm b})$ is obtained by recording the number of rising edges of the pulse train and it can not exceed $k_{\max}=\lfloor T_{\rm b}/\tau\rfloor+1$, where $\lfloor x\rfloor$ denotes the largest integer that is smaller than x.

A. AQ SPAD

For AQ SPADs, after each photon detection, the detector is inactive for a constant time τ. A photon is detected if and only if no detection event has taken place during a time τ preceding it, and any photon arriving during the dead time is neither counted nor has any influence on the dead time duration.

Theorem 2: The photocount distribution of an AQ SPAD with nonparalyzable dead time of τ, during the time interval of $(0,T_{\rm b})$ is given by:

$$p_K(k)=\sum_{i=0}^{k}\psi(i,\lambda_{k+1})-\sum_{i=0}^{k-1}\psi(i,\lambda_k)\,, \tag{27}$$

for $k<k_{\max}$. Function $\psi(i,\lambda)$ is defined as $\psi(i,\lambda)=\lambda^i e^{-\lambda}/i!$, and $\lambda_k=\lambda(T_{\rm b}-k\tau)$.

Proof: Assuming $\tau_2=0$ in (16), the photocount distribution for an AQ SPAD is obtained:

$$\begin{aligned}p(k,t)&=\sum_{r=0}^{\infty}(-1)^r\binom{k+r-1}{r}\frac{\lambda^{k+r}(t-k\tau)^{k+r}}{(k+r)!}\\&\quad-\sum_{r=0}^{\infty}(-1)^r\binom{k+r}{r}\frac{\lambda^{k+r+1}(t-(k+1)\tau)^{k+r+1}}{(k+r+1)!},\end{aligned} \tag{28}$$

for $k<k_{\max}$, and $p(k,t)=0$ for $k\geq k_{\max}$. Note that in (16) normalized photon arrival rate (i.e. $\lambda=1$) was assumed and in (28) this assumption is released. The expression for $p(k,t)$ can be further simplified to:

$$\begin{aligned}p(k,t)&=\sum_{i=0}^{k}\frac{\lambda^i(t-(k+1)\tau)^i}{i!}e^{-\lambda(t-(k+1)\tau)}\\&\quad-\sum_{i=0}^{k-1}\frac{\lambda^i(t-k\tau)^i}{i!}e^{-\lambda(t-k\tau)}\,.\end{aligned} \tag{29}$$

Hence, $p_K(k)=p(k,t)|_{t=T_{\rm b}}$ and the theorem follows. ■

The above expression is in line with results previously derived in [24], [26]. The probability mass function (PMF) obtained in (27) is plotted in Fig. 1 and compared with Monte Carlo simulation results for different values of dead time ratio, $\delta=\tau/T_{\rm b}$. In this figure, a time interval of $T_{\rm b}=1$ μs is considered and $\lambda=3\times10^7$ photons/s. Also, $\delta=0$, 0.02, 0.05, and 0.07 are assumed. Note that for a receiver without dead time, the photocount distribution is Poisson with mean $\lambda T_{\rm b}$. For the PMF expression in (27), some of the main properties shall be addressed as follows:

1) The unitary condition: As required for any valid distribution function, for the PMF in (27), the equality $\sum\limits_k p_K(k)=1$ holds. Furthermore, it is easily seen that $\lim_{\tau\to0}p_K(k)=p_0(k)$, that is, when τ goes to zero, the original Poisson distribution is recovered.

2) First and second moments:

Proposition 3: The mean and variance of the photocount distribution in (27) are:

$$\mu_K=(k_{\max}-1)-\sum_{k=0}^{k_{\max}-2}\sum_{i=0}^{k}\psi(i,\lambda_{k+1}), \tag{30}$$

This article has been accepted for publication in a future issue of this journal, but has not been fully edited. Content may change prior to final publication. Citation information: DOI 10.1109/TCOMM.2018.2822815, IEEE Transactions on Communications

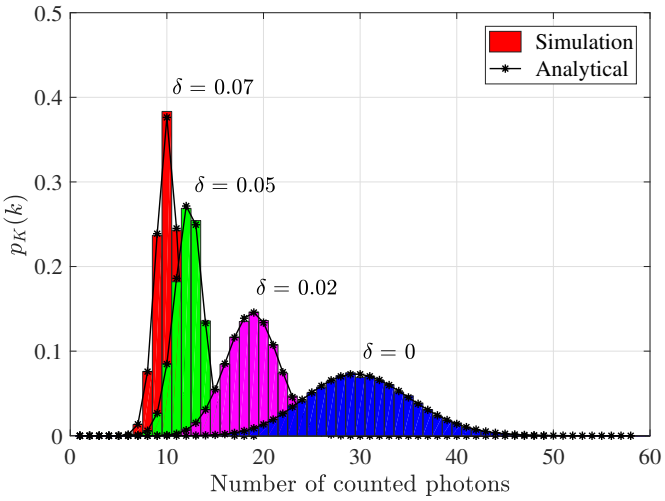

Fig. 1. Probability distribution of AQ SPAD photocounts for $T_\mathrm{b} = 1$ μs, $\lambda = 3 \times 10^7$ photon/s and different values of δ.

$$\sigma_K^2 = \sum_{k=0}^{k_{\max}-2} \sum_{i=0}^{k} (2k_{\max} - 2k - 3)\psi(i, \lambda_{k+1}) - \left(\sum_{k=0}^{k_{\max}-2} \sum_{i=0}^{k} \psi(i, \lambda_{k+1}) \right)^2. \tag{31}$$

Proof: Please refer to Appendix B. ■

Again, as dead time goes to zero, the limiting relations $\lim_{\tau \to 0} \mu_K = \lambda T_\mathrm{b}$ and $\lim_{\tau \to 0} \sigma_K^2 = \lambda T_\mathrm{b}$ in (30) and (31) can be verified, where λT_b is the mean value of the ideal Poisson distribution.

Fig. 2a presents μ_K and σ_K^2 for an AQ SPAD as functions of λ where they are compared to an ideal Poisson counting process. As shown, the difference between μ_K and σ_K^2 becomes more significant as λ increases. Let the ratio of the variance to mean be defined as:

$$\xi = \frac{\sigma_K^2}{\mu_K}. \tag{32}$$

Fig. 2b illustrates this ratio where it approaches to zero as λ goes to infinity, unlike the Poisson distribution where this ratio is equal to one for all values of λ.

3) Asymptotic mean for large T_b/τ ratio: The exact mean value in (30) can also be expressed as follows:

$$\mu_K = (k_{\max} - 1) - \sum_{k=0}^{k_{\max}-2} \frac{\Gamma(k+1, \lambda_{k+1})}{\Gamma(k+1)}, \tag{33}$$

where for a positive integer s, $\Gamma(s) = (s-1)!$ and $\Gamma(s,x) = e^{-x}(s-1)! \sum_{i=0}^{s-1} \frac{x^i}{i!}$ are the gamma function and incomplete gamma function, respectively [30]. Defining $\gamma(s,x) = \Gamma(s,x)/\Gamma(s)$, the following approximation holds for $\gamma(k+1, \lambda_{k+1})$ when T_b/τ goes to infinity [30]:

$$\gamma(k+1, \lambda_{k+1}) \approx \begin{cases} 1, & k+1 > \lambda_{k+1} \\ 0, & k+1 \leq \lambda_{k+1} \end{cases}.$$

Therefore, $\gamma(k+1, \lambda_{k+1})$ can be approximated as zero for $k \leq (\lambda T_\mathrm{b} - \lambda\tau - 1)/(1+\lambda\tau)$, and 1, otherwise. Applying the above approximation to (33) gives:

$$\lim_{T_\mathrm{b}/\tau \to \infty} \mu_K = \frac{\lambda T_\mathrm{b}}{1+\lambda\tau}. \tag{34}$$

Thus, the asymptotic count rate of an AQ SPAD, i.e. the average number of recorded photons per second, is given by:

$$\lambda' = \frac{\lambda}{1+\lambda\tau}. \tag{35}$$

This expression is in line with the asymptotic expressions presented in [31] and the practical models provided in [22].

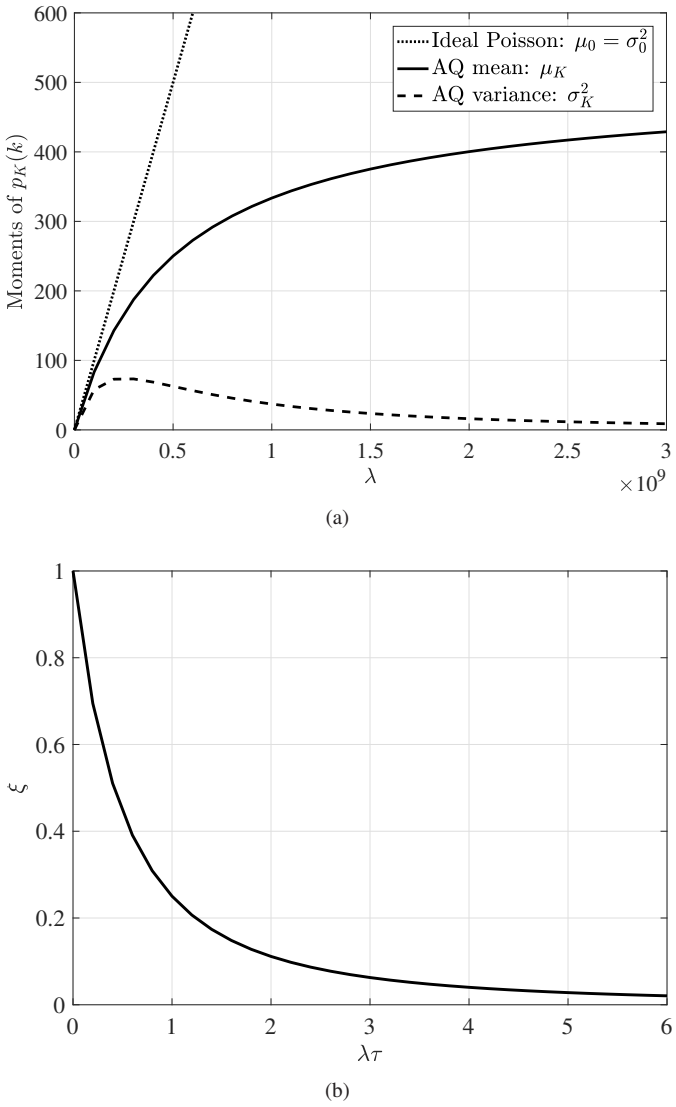

Fig. 2. First and second moments of AQ SPAD photocounts with $T_\mathrm{b} = 1$ μs, $\tau = 2$ ns: (a) comparison of mean and variance with ideal Poisson distribution, (b) the variance to mean ratio.

B. PQ SPAD

For PQ SPADs, any photon arrival is followed by dead time, and the ones occurring during the dead time of previous photons, extend the dead time duration.

Theorem 4: The photocount distribution of a PQ SPAD with paralyzable dead time of τ, during the time interval of

This article has been accepted for publication in a future issue of this journal, but has not been fully edited. Content may change prior to final publication. Citation information: DOI 10.1109/TCOMM.2018.2822815, IEEE Transactions on Communications

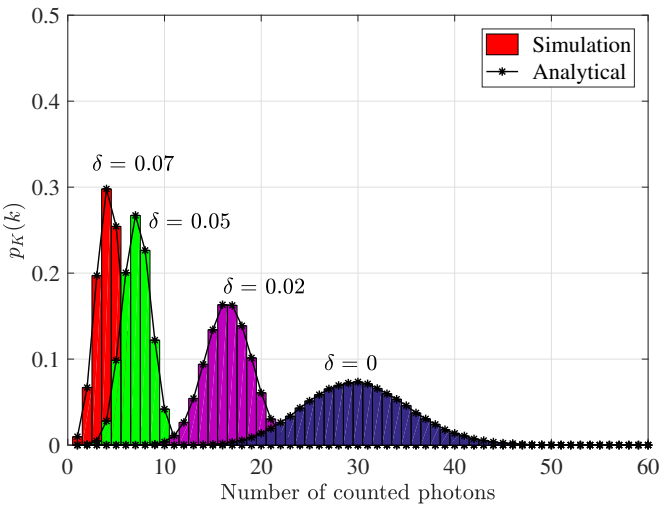

Fig. 3. Probability distribution of PQ SPAD photocounts for $T_\mathrm{b} = 1$ μs, $\lambda = 3 \times 10^7$ photon/s and different values of δ.

$(0, T_\mathrm{b})$ is given by:

$$p_K(k) = \sum_{i=k}^{k_{\max}-1} (-1)^{i-k} \binom{i}{k} \frac{\lambda^i (T_\mathrm{b} - i\tau)^i}{i!} e^{-i\lambda\tau} , \quad (36)$$

for $k < k_{\max}$ and $p_K(k) = 0$ for $k \geq k_{\max}$.

Proof: Assuming $\tau_1 = \tau_2 = \tau$ in (16), the photocount distribution for a PQ SPAD is obtained which is further simplified to:

$$p(k,t) = \sum_{r=0}^{K} (-1)^r \binom{k+r}{r} \frac{\lambda^{k+r}(t-(k+r)\tau)^{k+r}}{(k+r)!} e^{-(k+r)\lambda\tau} . \quad (37)$$

With a change of variable $i = k + r$:

$$p(k,t) = \sum_{i=k}^{K+k} (-1)^{i-k} \binom{i}{k} \frac{\lambda^i (t - i\tau)^i}{i!} e^{-i\lambda\tau} . \quad (38)$$

where K is an integer such that:

$$\frac{t}{\tau} - (k+1) < K < \frac{t}{\tau} - k$$

With $p_K(k) = p(k,t)|_{t=T_\mathrm{b}}$, and therefore $K + k = k_{\max} - 1$, the expression in (36) is obtained. Hence, the theorem follows. ■

The PMF obtained in (36) is plotted in Fig. 3 and compared with the Monte Carlo simulation results for different values of $\delta = \tau/T_\mathrm{b}$. In Fig. 3, a time interval of $T_\mathrm{b} = 1$ μs is considered and $\lambda = 3 \times 10^7$ photons/s. Also, $\delta = 0$, 0.02, 0.05, and 0.07 are assumed. Note that for a receiver without dead time, the photocount distribution is Poisson with mean λT_b. For the PMF expression in (36), some of the main properties are addressed as follows:

1) The unitary condition: It can easily be verified that the unitary condition $\sum_{k=0}^{\infty} p_K(k) = 1$ holds for the PMF in (36) and $\lim_{\tau\to 0} p_K(k) = p_0(k)$, that is, when τ goes to zero, the PMF in (36) approaches the ideal Poisson distribution.

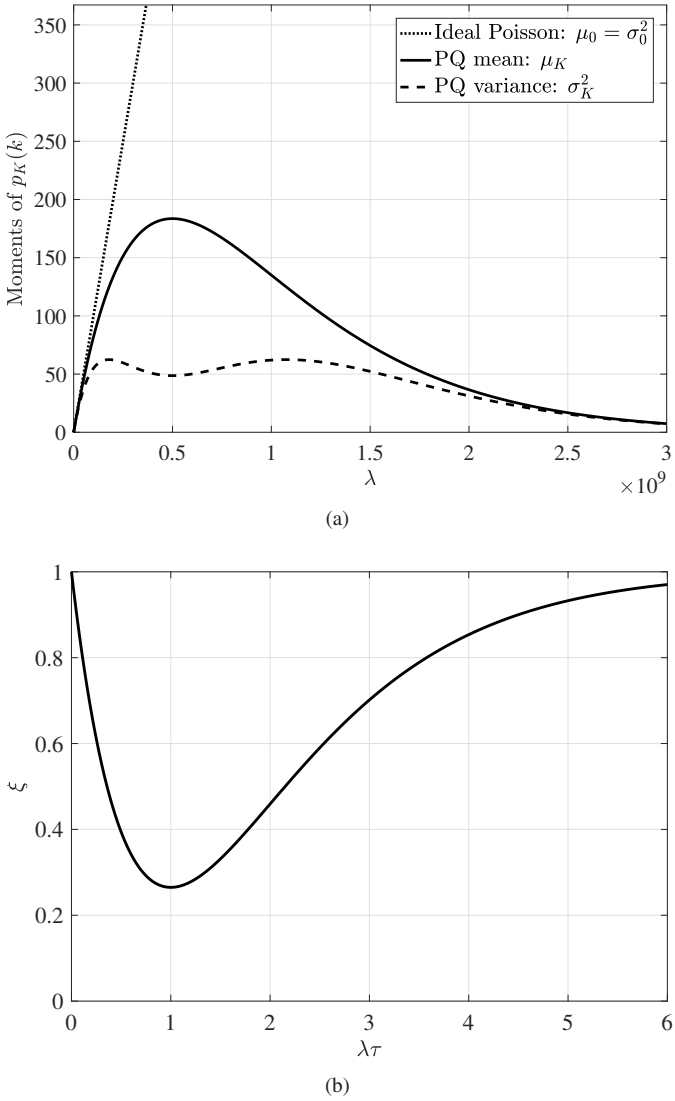

Fig. 4. First and second moments of PQ SPAD photocounts with $T_\mathrm{b} = 1$ μs, $\tau = 2$ ns: (a) comparison of mean and variance with ideal Poisson distribution, (b) the variance to mean ratio.

2) First and second moments:

Proposition 5: The mean and variance of the photocount distribution in (36) are derived as:

$$\mu_K = \lambda e^{-\lambda\tau}(T_\mathrm{b} - \tau), \quad (39)$$

$$\sigma_K^2 = \lambda^2 e^{-2\lambda\tau}(3\tau^2 - 2T_\mathrm{b}\tau) + \lambda e^{-\lambda\tau}(T_\mathrm{b} - \tau). \quad (40)$$

Proof: Please refer to Appendix C. ■

Similar to AQ SPAD, the limiting relations $\lim_{\tau\to 0} \mu_K = \lambda T_\mathrm{b}$ and $\lim_{\tau\to 0} \sigma_K^2 = \lambda T_\mathrm{b}$ in (39) and (40) can be confirmed, where λT_b is the mean value of the ideal Poisson distribution (see Appendix C). Fig. 4a presents μ_K and σ_K^2 for a PQ SPAD as functions of λ. The mean and variance are also compared to an ideal counting process where it is observed that unlike a Poisson process, μ_K and σ_K^2 can differ greatly. Fig. 4b illustrates the ratio, ξ, as defined in (32) where the minimum occurs at $\lambda\tau = 1$ and the ratio approaches 1 when $\lambda\tau$ goes to infinity.

3) Asymptotic mean for large $T_{\rm b}/\tau$ ratio: For the case when the ratio $T_{\rm b}/\tau$ is large, yet the dead time cannot be ignored, the following asymptotic expression for mean value is obtained:

$$\lim_{T_{\rm b}/\tau\to\infty} \mu_K = \lambda T_{\rm b} e^{-\lambda\tau}. \tag{41}$$

Therefore, the asymptotic count rate of a PQ SPAD, i.e. the average number of recorded photons per second, is given by:

$$\lambda' = \lambda e^{-\lambda\tau}. \tag{42}$$

This expression is in line with the asymptotic expressions presented in [31] and the practical models provided in [22].

IV. SPAD-based Optical Communication Systems

SPADs have been used as photon counting receivers in OWC systems [7], [17], [19], [20]. Free space optics (FSO), visible light communications (VLC), wireless IR, deep space communications are all examples of such OWC applications. In this section the effect of dead time on the bit error performance of a SPAD-based optical system with on-off keying (OOK) and binary pulse position modulation (BPPM) is studied. The SPAD's dead time also limits the maximum achievable data rate of the system. The dead time of commercially available SPAD devices varies in the range of a few nanoseconds to tens of nanoseconds. Using binary modulation schemes, a reliable bit error performance with maximum data rate of a few Mbits/s can be achieved. For example, with OOK modulation, the highest data rate to be achieved by an AQ SPAD with dead time τ can not exceed $1/\tau$, and this is due to saturation of SPAD receiver [26]. For a PQ SPAD receiver the maximum achievable data rate is even lower than $1/\tau$. Note that the maximum achievable data rate depends on not only the dead time, but also the operating conditions [28]. Throughout this paper, a data rate of 1 Mbits/s is assumed.

In the following, the bit error performance of a SPAD-based optical system with OOK and BPPM is derived. In these binary modulation schemes, each bit is sent individually by transmitting one of two optical pulses over a duration of $T_{\rm b}$ seconds and the optical intensity modulated signal is transmitted by an optical source. In this system the bit rate is expressed as $R_{\rm b} = 1/T_{\rm b}$ bits/s. At the receiver side, direct detection is applied where the received optical signal is photodetected by the SPAD. The number of photons counted by the SPAD is processed to decide which of two optical pulses was received, and then the transmitted bit during each $T_{\rm b}$ second bit interval is determined. In this photon counting system, the background counts and the SPAD's dead time determine the achievable bit error ratio (BER) of the system.

A. On-Off Keying

OOK is one of the most common modulation techniques for intensity-modulation direct-detection (IM/DD) systems, because of its easy implementation, simple receiver design, bandwidth efficiency and cost effectiveness. In OOK, the information bits are transmitted through the intensity of light, where presence of a pulse denotes bit "1" and absence of a pulse denotes bit "0", during each slot time.

Define the contributions to the signal and background noise counts per bit interval by $K_{\rm s} = \lambda_{\rm s} T_{\rm b}$ and $K_{\rm n} = \lambda_{\rm n} T_{\rm b}$, respectively, where $\lambda_{\rm s}$ and $\lambda_{\rm n}$ are the average photon rates from signal and background noise. When a "0" bit is transmitted, the average number of photons arrived at the SPAD receiver per bit time interval is $K_{\rm n}$, and when a "1" bit is transmitted, the average number of received photons per bit time interval is $K_{\rm s} + K_{\rm n}$. Therefore, $p_{\rm n}(k)$ and $p_{\rm sn}(k)$, the probability that exactly k photons are counted by the SPAD in the counting interval of $T_{\rm b}$ seconds, when "0" or "1" are sent, respectively, are given by:

$$\begin{aligned} p_{\rm n}(k) &= p_K(k; \lambda_{\rm n}, T_{\rm b}, \tau)\ , \\ p_{\rm sn}(k) &= p_K(k; \lambda_{\rm s} + \lambda_{\rm n}, T_{\rm b}, \tau)\ . \end{aligned} \tag{43}$$

OOK demodulation is accomplished by a classical binary detection process: Let hypothesis "H_0" represent the case when a "0" is sent and "H_1" represent the hypothesis that a "1" is transmitted. The aim is to determine the optimum rule for deciding which hypothesis is true based on a single observation. This simple binary hypothesis-testing problem is often formulated using the Bayes criterion, where the decision should be made according to the well-known likelihood-ratio test to minimize the probability of error. In this test, the likelihood ratio is defined as:

$$L(k) = \frac{p_{\rm sn}(k)}{p_{\rm n}(k)} \underset{H_0}{\overset{H_1}{\gtrless}} 1 \tag{44}$$

where it is assumed that H_0 and H_1 are equally probable. With this maximum likelihood detection rule, the probability of error is expressed as:

$$P_e = \frac{1}{2} \sum_{\{k:L(k)>1\}} p_{\rm n}\left(k\right) + \frac{1}{2} \sum_{\{k:L(k)\le 1\}} p_{\rm sn}\left(k\right)\ . \tag{45}$$

For an ideal photon detector with Poisson statistics (without dead time), the likelihood-ratio test in (44) simplifies to a single threshold detection. For the SPAD receiver, however, the complicated mathematical expressions of $p_{\rm sn}(k)$ and $p_{\rm n}(k)$ (for both AQ and PQ SPADs), makes the algebraic manipulation of $L(k)$ intractable. For given values of $\lambda_{\rm s}$ and $\lambda_{\rm n}$, if $L(k)$ is monotonic with respect to k, the test in (44) is equivalent to a single threshold test, i.e. the maximum likelihood detection is achieved by a threshold comparison. But it is even more challenging to check the monotonicity of $L(k)$ using finite differences (discrete derivatives). For an AQ SPAD with small dead time ratio ($\delta < 0.1$), an approximate photocount distribution can be provided (see Appendix A) and it can be proved that the above likelihood-ratio test leads to a single threshold test (see Appendix D). For other cases, no such proof can be provided. However, we conjecture that the threshold detection is optimum in general. Our extensive numerical investigation of the monotonicity of $L(k)$ and and the BER results in Section V strongly support this conjecture.

Hereinafter, the threshold detection is adopted for error probability calculations, where the number of counted photons is compared with a threshold $m_{\rm T}$. An error will occur if $k \le m_{\rm T}$ when a "1" bit is sent, or if $k > m_{\rm T}$, when a "0" bit

is sent. The probability of error for equally likely bits is then expressed as:

$$P_e = \frac{1}{2}\sum_{k=m_{\rm T}+1}^{k_{\max}} p_{\rm n}(k) + \frac{1}{2}\sum_{k=0}^{m_{\rm T}} p_{\rm sn}(k)\ . \tag{46}$$

This equation holds for both AQ and PQ SPADs, however, for each case, the corresponding photocount distribution should be considered. The error probability, P_e, highly depends on $m_{\rm T}$ which can be selected to yield the lowest probability of making an error. This occurs at the value of $m_{\rm T}$ where $dP_e/dm_{\rm T} = 0$. It is in general challenging to obtain a closed-form expression for (46), nevertheless, for the case of an AQ SPAD, it is shown that (see Appendix E) given same conditions (i.e. same threshold, sampling time, and radiation intensity), the error performance of an AQ SPAD with dead time is the same as that of a similar SPAD without dead time, but with a quantum efficiency reduced by the factor $(1-(m_{\rm T}+1)\tau/T_{\rm b})$. According to (66):

$$\begin{aligned} P_e = \frac{1}{2}\left(1-\sum_{k=0}^{m_{\rm T}}\psi(k,\lambda_{\rm n}(T_{\rm b}-(m_{\rm T}+1)\tau))\right) \\ + \frac{1}{2}\sum_{k=0}^{m_{\rm T}}\psi(k,(\lambda_{\rm s}+\lambda_{\rm n})(T_{\rm b}-(m_{\rm T}+1)\tau))\ . \end{aligned} \tag{47}$$

Solving the equation $dP_e/dm_{\rm T} = 0$ for finding the optimum threshold value leads to:

$$m_{\rm T} = \frac{\lambda_{\rm s}T_{\rm b}-\lambda_{\rm s}\tau}{\lambda_{\rm s}\tau+\ln\left(1+\frac{\lambda_{\rm s}}{\lambda_{\rm n}}\right)}\ . \tag{48}$$

B. Binary Pulse Position Modulation

The basic disadvantage of OOK signaling is that the average photon rates $\lambda_{\rm s}$ and $\lambda_{\rm n}$ must be known, to optimally set the threshold. BPPM signaling avoids this difficulty by using pulse-to-pulse comparison for detection. In BPPM modulation, the optical pulse is sent in one of two adjacent time intervals, each of length $T_{\rm b}/2$ and then the output counts are compared over each half-bit interval. A "1" bit is sent as a pulse in the first half of the bit interval, and a "0" bit as a pulse in the second half. At the receiver side, the SPAD separately counts the number of photons over the two half-bit intervals and then they are compared for bit decoding. Since the pulse time is half of the bit duration, the receiver bandwidth must be higher than for the OOK system [1].

With the same approach as used for OOK, the bit error probability of the BPPM system is the probability that signal slot photon count does not exceed non-signal slot photon count. Hence:

$$P_e = \sum_{k_1=0}^{\infty}\sum_{k_2=k_1+1}^{\infty} p_{\rm sn}(k_1)p_{\rm n}(k_2) + \frac{1}{2}\sum_{k=0}^{\infty} p_{\rm sn}(k)p_{\rm n}(k)\ . \tag{49}$$

where the second term in (49) accounts for the possibility of equal counts in each half-bit interval, in which case a random choice will be made.

V. Numerical Results and Discussion

In this section, bit error performance results are presented where analytical results are compared with Monte Carlo simulation results. Throughout the calculations and simulations, independent count statistics are assumed for each transmitted bit and $T_{\rm b} = 1\ \mu$s is considered. In all figures, BER results are plotted as a function of $\overline{K_{\rm s}}$ for various $\overline{K_{\rm n}}$ values and $\delta = \tau/T_{\rm b}$, where $\overline{K_{\rm s}}$ and $\overline{K_{\rm n}}$ are defined as the average signal count and background count per bit interval, respectively. Therefore, for both OOK and BPPM, $\overline{K_{\rm s}} = 0.5\lambda_{\rm s}T_{\rm b}$ and $\overline{K_{\rm n}} = 0.5\lambda_{\rm n}T_{\rm b}$.

A. AQ SPAD

The BER results for an AQ SPAD-based optical system with OOK modulation are provided in Fig. 5. In these figures, the error probability of OOK systems with maximum likelihood (ML) detection and threshold (TH) detection are compared with Monte Carlo simulation results, resulting in perfectly matching curves. The analytical calculations are based on the expressions given in (45) for ML detection, and (47) and (48) for TH detection.

According to Figs. 5a and 5b, ML and TH detection show an excellent match for all cases, confirming that for the specified range of values in these figures, the ML detection and TH detection are equivalent.

In Fig. 5a, moderately small values of $\delta = 0.001$ and $\delta = 0.01$ are assumed, while in Fig. 5b the dead time ratio is $\delta = 0.1$ which is quite large for communication purposes. As observed in Fig. 5b, the large value of dead time ratio degrades the system performance as the SPAD is saturated with lower signal and/or background noise levels. In these cases, $k_{\max}$ and $m_{\rm T}$ are small, and the ripples in the BER curves are direct results of discrete threshold values. For the quantum-limited cases, i.e. $\overline{K_{\rm n}} = 0$ curves, the threshold $m_{\rm T}$ is zero and no ripples are observed.

According to Fig. 5a, the performance of the AQ SPAD receiver depends strongly on the background count statistics, and even for $\overline{K_{\rm n}} = 0$ and 1, the error probability is slightly affected by the SPAD dead time. This becomes more significant, when $\overline{K_{\rm n}}$ increases. Also, it is apparent that for a given $\overline{K_{\rm n}}$, a higher signal power is needed to maintain the system performance in the presence of longer dead time. In other words, to achieve a particular BER, the larger δ is, the higher $\overline{K_{\rm s}}$ should be.

Fig. 6 provides the BER results for an AQ SPAD-based optical system with BPPM modulation. It is observed that, in the absence of background noise, the effect of dead time on BER is negligible for small values of $\overline{K_{\rm s}}$ as in Fig. 6a. However, when background noise is present, the performance becomes very sensitive to the dead time such that higher dead time values lead to higher error rates. It should also be noted that, as seen in Fig. 6b, the error performance severely degrades when large dead time ratio ($\delta = 0.1$) is assumed. In this case, the SPAD gets saturated with lower signal and/or background noise levels. Also, for stronger background counts, the saturation happens at lower signal levels.

This article has been accepted for publication in a future issue of this journal, but has not been fully edited. Content may change prior to final publication. Citation information: DOI 10.1109/TCOMM.2018.2822815, IEEE Transactions on Communications

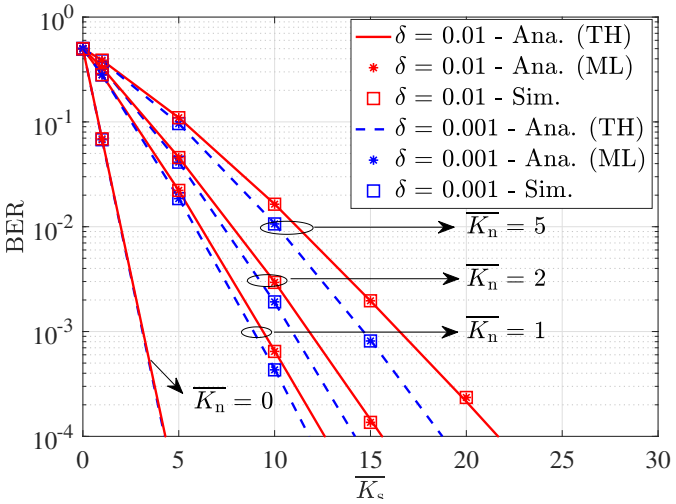

(a)

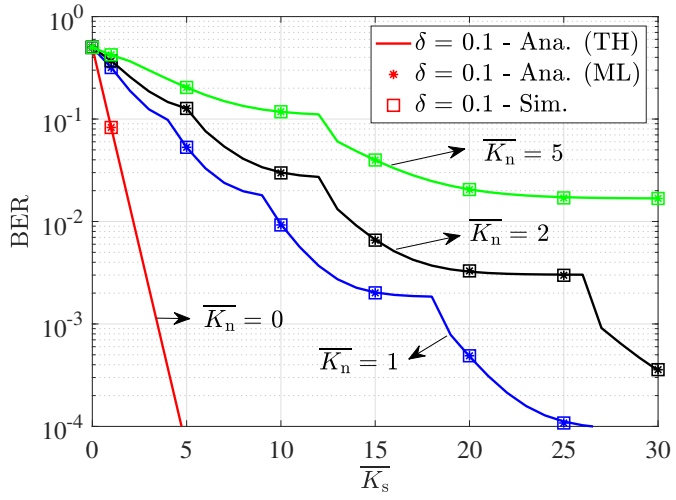

(b)

Fig. 5. OOK bit error performance of an AQ SPAD-based system: (a) $\delta = 0.01, 0.001$ and (b) $\delta = 0.1$.

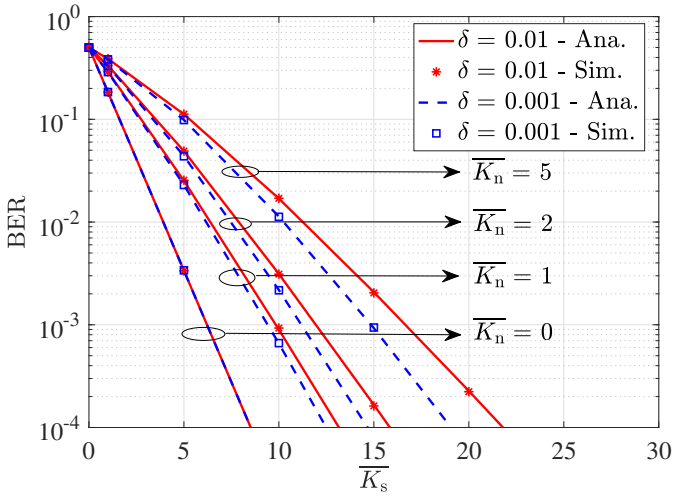

(a)

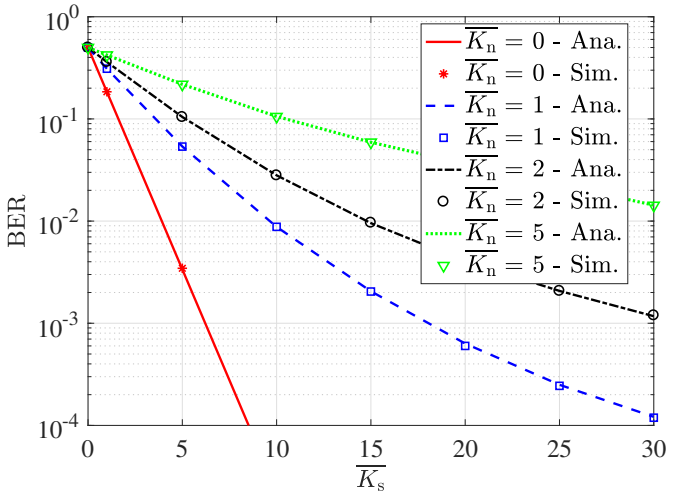

(b)

Fig. 6. BPPM bit error performance of an AQ SPAD-based system: (a) $\delta = 0.01, 0.001$ and (b) $\delta = 0.1$.

Note that OOK uses pulses twice as long as BPPM, and has higher signal and background counts. Therefore, a fair comparison between OOK and BPPM systems can be made if the same average signal and background power are assumed. For the systems under consideration, average signal and background noise power are directly proportional to $\overline{K_s}$ and $\overline{K_n}$, respectively. Thus, it is fair to compare the error performance of OOK and BPPM systems as presented in Figs. 5 and 6.

As in Fig. 5a and Fig. 6a, OOK and BPPM show almost similar performance when the background noise is present and the dead time ratio is moderately small. For large dead time ratio ($\delta = 0.1$ as in Fig. 5b and Fig. 6b), in the presence of background counts, OOK system shows slightly better BER values. For ideal quantum-limited photon-counting OOK and BPPM ($\overline{K_n} = 0$) without dead time counting losses, OOK has 3 dB better performance as discussed in [1]. In the presence of dead time, consistent results are achieved, however, the effect of dead time is insignificant in the range of interest as illustrated in Figs. 5 and 6.

B. PQ SPAD

Fig. 7 demonstrates the error performance results of a PQ SPAD-based system with OOK modulation. In this figure, the error probability with ML detection, given in (45), and the error probability with TH detection, given in (46) are numerically evaluated and compared with simulation results. The threshold value is also obtained numerically. It is again observed that ML and TH detection rules result in perfectly matching curves, confirming that these two detection schemes are equivalent in the range of interest.

Similar to BER results for the AQ SPAD, three different values for dead time ratio are considered here. In Fig. 7a, $\delta = 0.001$ and $\delta = 0.01$ are assumed, while in Fig. 7b the dead time ratio is equal to 0.1. Again, large dead time ratio ($\delta = 0.1$) severely degrades the error performance and results in SPAD's saturation. According to (42), for a PQ SPAD, the maximum count rate occurs at the point $\lambda = 1/\tau$. The lowest BER also occurs at this point which is clearly seen in Fig. 7b. After this point, the counting losses due to

This article has been accepted for publication in a future issue of this journal, but has not been fully edited. Content may change prior to final publication. Citation information: DOI 10.1109/TCOMM.2018.2822815, IEEE Transactions on Communications

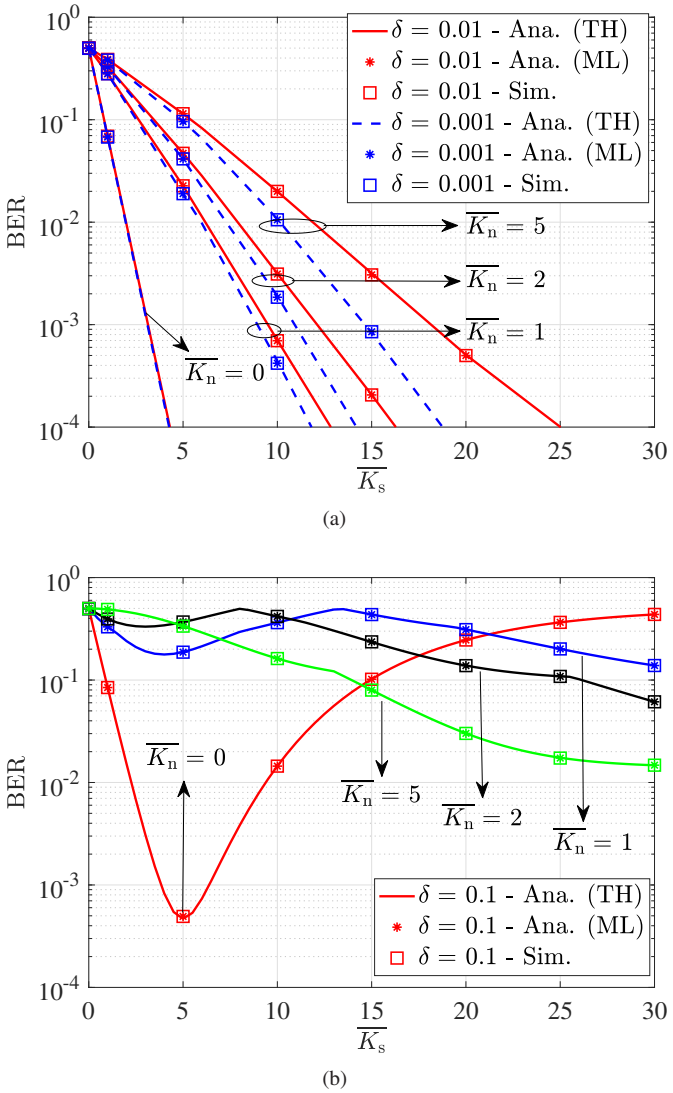

Fig. 7. OOK bit error performance of a PQ SPAD-based system: (a) $\delta = 0.01, 0.001$ and (b) $\delta = 0.1$.

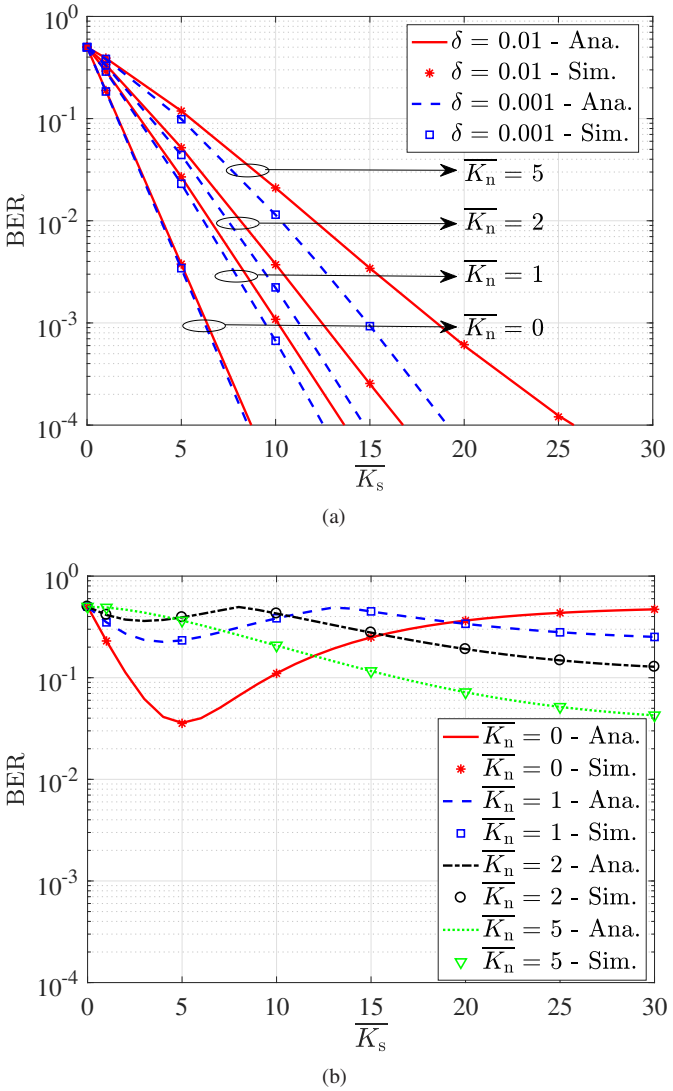

Fig. 8. BPPM bit error performance of a PQ SPAD-based system: (a) $\delta = 0.01, 0.001$ and (b) $\delta = 0.1$.

dead time drastically increase. The BER also increases until the paralysis behaviour (see Fig. 4) results in the average photon count of pulsed slots becoming lower than that of non-pulsed slots. Our extensive numerical calculations show that at this latter point, the monotonicity of the likelihood ratio function $L(k)$, given in (44) changes from monotonically nondecreasing to monotonically nonincreasing. In such cases, keeping the definition of hypotheses H_0 and H_1 as before, the direction of the likelihood ratio test presented in (44) should be reversed and the error probability expressions should be modified accordingly. This has been done for obtaining the results of Fig. 7b.

The probability of error for a PQ SPAD-based optical system with BPPM modulation, given in (49), is in the form of discrete summations, and therefore can be calculated numerically. Fig. 8 shows some plots of the BER results for such a system. Similar to previous cases, in the absence of background noise, the effect of dead time on BER is almost negligible. However, an increase in the dead time value degrades the error performance. Again, it is seen that the error performance is severely affected by large dead time ratio ($\delta = 0.1$) and the lowest BER occurs at the maximum count rate, as predicted.

As seen in Figs. 5–8, the BER of the OWC system strongly depends on the value of dead time and large dead time values increase the BER to levels even beyond 10^{-3}. The dead time of commercially available SPAD devices vary in the range of a few nanoseconds to tens of nanoseconds, causing significant losses for communication links with slot widths of the same order. However, for data rates in the orders of a few tens of Mbits/s and lower, the dead time ratio is small enough (≤ 0.01) and assuming binary modulation schemes such as OOK and BPPM, BER values of less than 10^{-3} can be achieved, as shown in Figs. 5a, 6a, 7a and 8a for AQ and PQ cases, respectively. These results highlight the need to develop SPAD detectors with much reduced dead time to be able to achieve higher data rates with reliable performance and arbitrary small bit error probability.

This article has been accepted for publication in a future issue of this journal, but has not been fully edited. Content may change prior to final publication. Citation information: DOI 10.1109/TCOMM.2018.2822815, IEEE Transactions on Communications

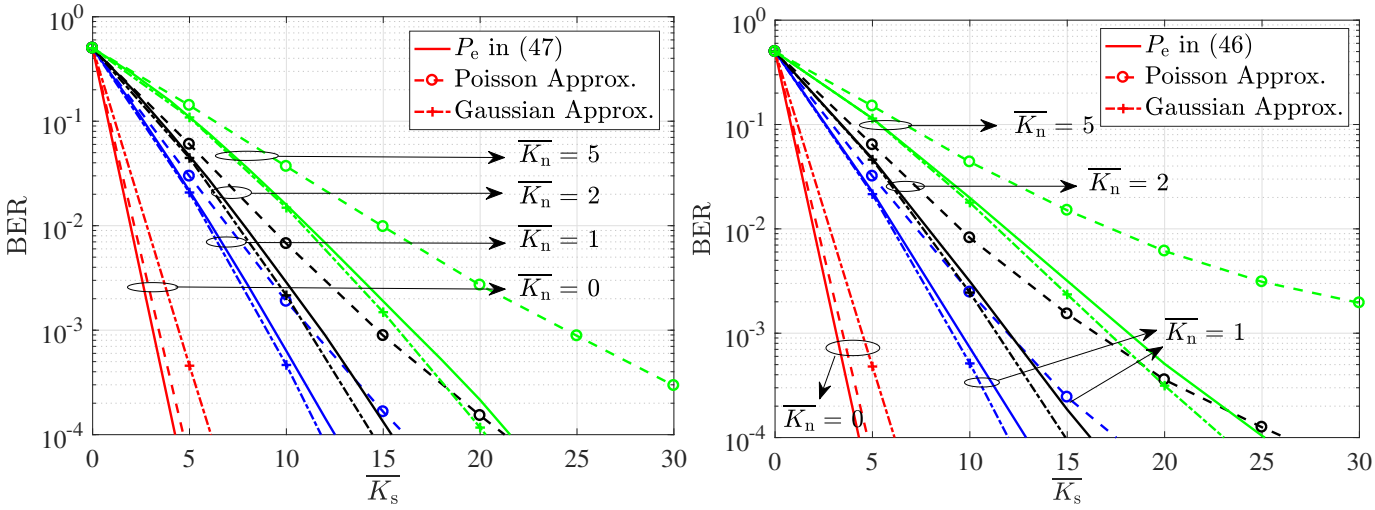

(a) AQ (b) PQ

Fig. 9. BER performance of (a) AQ, and (b) PQ SPAD-based systems with OOK modulation considering exact SPAD photocount distribution, Poisson approximation, and Gaussian approximation.

C. AQ SPAD vs. PQ SPAD

As stated in Section I, when using PQ SPADs any photon arrival occurring during the dead time is not counted but is assumed to extend the dead time period, while for AQ SPAD devices, any photon arriving during the dead time is neither counted nor has any influence on the dead time duration. Thus, assuming the same dead time duration, in a bit interval of T_b seconds, the average number of counted photons by an AQ SPAD is generally higher than that of a PQ SPAD. This can be observed from Figs. 1 and 3. Furthermore, this behavior directly affects the BER performance. When the dead time duration only is one order of magnitude lower than the bit interval ($\delta = 0.1$), the difference of AQ and PQ SPADs is perceptible, as observed in Fig. 5b and Fig. 7b for OOK modulation or in Fig. 6b and Fig. 8b for BPPM. For an AQ SPAD, increasing the signal photon rate (or signal count) results in the saturation of SPAD and the BER will reach a constant value. However, in a PQ SPAD, by increasing the signal photon rate (or signal count), the BER decreases until the SPAD reaches its maximum count rate. At this point, the lowest possible BER is achieved and higher signal counts degrade the error performance.

D. Applicability of Gaussian and Poisson Approximations

The probability distribution of SPAD photocounts is commonly approximated by a Poisson distribution where the effect of dead time is neglected. In order to investigate the accuracy of this approximation, in Fig. 9, the OOK error probabilities of both AQ and PQ SPADs, given in (47) and (46), respectively, are evaluated and compared with the case when the photocount distribution is approximated by a Poisson distribution through moment matching, i.e., the rate parameter of the approximated Poisson distribution is calculated according to (35) and (42) as in [7], [8], rather than using an ideal Poisson model which does not take into account the effect of dead time. Please note that in Figs. 9a and 9b, $\delta = 0.01$ is assumed, and as can be seen, for both AQ and PQ SPADs, there is a considerable difference between the exact BER values and the Poisson approximation results, especially for higher values of $\overline{K_n}$.

To have a better insight, the AQ and PQ SPAD photocount distributions have also been approximated by Gaussian distribution in Fig. 9, using a similar moment matching approach. The mean and variance of the Gaussian distribution are approximated as in (30) and (31) for AQ SPAD, and as in (39) and (40) for PQ SPAD. Although the Gaussian approximation shows higher accuracy compared with the Poisson approximation, the differences are still noticeable. Note that by increasing the dead time ratio, the accuracy of these approximations will be more degraded. By comparing the results of these approximations for AQ and PQ SPADs, it is observed that the approximations show slightly higher accuracy for AQ SPADs, and the reason is that the counting losses due to paralyzable dead time are generally higher than that of nonparalyzable dead time. According to these observations, the use of Poisson or Gaussian approximations does not provide enough accuracy for assessing the bit error performance of OWC systems, and this highlights the importance of our statistical modeling for a precise bit error analysis for potential optical communication applications.

VI. Conclusions and Future Works

In this paper, a complete analytical framework is presented for modeling the statistical behavior of photon counting receivers. This rigorous analysis expounds the impact of paralyzable and nonparalyzable dead times on the counting statistics of SPAD detectors, and provides exact expressions for the probability distribution, mean and variance of active and passive quenching SPAD photocounts. The proposed expressions for mean of AQ and PQ SPAD photocounts precisely predict the SPAD effective count rates and are in line with empirical count rate models and experimental data available in literature. The proposed probability distributions are particularly required

for maximum likelihood detection analysis and assessing the bit error performance of any SPAD-based OWC system. In this study, the effect of dead time on the bit error performance of an OWC system with OOK and BPPM modulation schemes is investigated and it is found that that the dead time-distorted count statistics result in higher bit error rates, and a higher signal intensity is required to maintain system performance. In the AQ SPAD-based OWC system, assuming OOK modulation and constant average background count of $\overline{K_{\rm n}} = 1$, for a BER value of 10^{-4}, the reduction of dead time by one order of magnitude leads to almost 3 dB improvement in the average signal count. The improvement is about 3.8 dB if BPPM modulation is considered. PQ SPAD-based OWC systems with large dead time ratios ($\delta = 0.1$) can not achieve BER values lower than 10^{-3}. In general, for large dead time values, AQ SPADs outperform PQ SPADs significantly, and for small dead time values, AQ SPADs still provide slightly better bit error performance. It is also found that in quantum-limited OWC systems, the effect of dead time is negligible. Compared with Gaussian and Poisson distributions commonly used in literature, our proposed probability distributions provide significant accuracy in performance analysis of OWC systems. This in turn highlights the importance of our statistical modeling for a precise bit error analysis for potential optical communication applications. Moreover, it is concluded that in applications involving high photon rates, such as high data rate optical wireless communications, the SPAD dead time causes significant data loss. Using commercially available SPAD devices with dead time values in the range of a few nanoseconds to tens of nanoseconds, a reliable bit error performance with maximum data rate of a few Mbits/s could be achieved through binary modulation schemes. Thus, this study highlights the need to develop SPAD devices with much reduced dead time to be able to achieve higher data rates in the range of Gbits/s.

There is much work yet to be done in the analysis of SPAD-based optical systems. It is of great importance to consider modulation schemes with higher spectral efficiencies and less sensitive to the fluctuations in the background and signal strengths. However, in higher order modulation schemes, the existence of dead time does not allow arbitrarily narrow time slots, as the SPAD's dead time can overlap two adjacent time slots. Therefore, for future works, the photocount statistics should be modified accordingly.

APPENDIX A
APPROXIMATE PMF FOR AQ SPADS WITH $\lambda \gg 1$ OR $\tau \ll T_{\rm b}$

The PMF in (27) can be re-written as:

$$\begin{aligned} p_K(k) &= \sum_{i=0}^{k} \psi(i,\lambda_{k+1}) - \sum_{i=0}^{k-1} \psi(i,\lambda_k) \\ &= \psi(k,\lambda_{k+1}) + \sum_{i=0}^{k-1} \big(\psi(i,\lambda_{k+1}) - \psi(i,\lambda_k)\big) \\ &= \psi(k,\lambda_{k+1}) \\ &\quad + \sum_{i=0}^{k-1} \psi(i,\lambda_{k+1}) \left[1 - \frac{(T_{\rm b}-k\tau)^i}{(T_{\rm b}-(k+1)\tau)^i} e^{-\lambda\tau}\right] . \end{aligned} \tag{50}$$

Define A and B as follows:

$$A = \sum_{i=0}^{k-1} \psi(i,\lambda_{k+1}) \underbrace{\left[1 - \frac{(T_{\rm b}-k\tau)^i}{(T_{\rm b}-(k+1)\tau)^i} e^{-\lambda\tau}\right]}_{B} .$$

Two asymptotic cases can be considered:

- $\lambda \gg 1$: The limiting relation $\lim_{t\to\infty} t^\alpha e^{-t} = 0$ results in $\lim_{\lambda\to\infty} A = 0$.
- $\tau \ll T_{\rm b}$: Since $\lim_{\delta\to 0} B = 0$ and $\psi(k,\lambda_{k+1})$ is finite, $\lim_{\delta\to 0} A = 0$ is concluded.

Therefore, for the above two cases, the following approximation can be adopted:

$$p_K(k) \approx \psi(k,\lambda_{k+1}) . \tag{51}$$

APPENDIX B
MEAN AND VARIANCE OF THE AQ PMF

By definition, the mean value of the distribution in (27) is:

$$\begin{aligned} \mu_K &= \sum_{k=0}^{k_{\max}-1} k\, p_K(k) \\ &= \sum_{k=0}^{k_{\max}-1} k \times \left\{ \sum_{i=0}^{k} \psi(i,\lambda_{k+1}) - \sum_{i=0}^{k-1} \psi(i,\lambda_k) \right\} . \end{aligned} \tag{52}$$

Replacing k by $k+1$ in the summation index of the second term in the right-hand side of the previous expression gives:

$$\begin{aligned} \mu_K &= \sum_{k=0}^{k_{\max}-1} \sum_{i=0}^{k} k\, \psi(i,\lambda_{k+1}) - \sum_{k=0}^{k_{\max}-2} \sum_{i=0}^{k} (k+1)\psi(i,\lambda_{k+1}) \\ &= \sum_{i=0}^{k_{\max}-1} (k_{\max}-1)\psi(i,\lambda_{k_{\max}}) - \sum_{k=0}^{k_{\max}-2} \sum_{i=0}^{k} \psi(i,\lambda_{k+1}) \\ &\approx (k_{\max}-1) - \sum_{k=0}^{k_{\max}-2} \sum_{i=0}^{k} \psi(i,\lambda_{k+1}) . \end{aligned} \tag{53}$$

where the approximation $\sum_{i=0}^{k_{\max}-1} \psi(i,\lambda_{k_{\max}}) \approx 1$ is used, as $\lambda_{k_{\max}}$ is very small. The above expression for μ_K in (53) can be further simplified to:

$$\mu_K = \sum_{k=0}^{k_{\max}-2} \sum_{i=k+1}^{\infty} \psi(i,\lambda_{k+1}) . \tag{54}$$

Next, the limit of this expression for $\tau \to 0$ or $k_{\max} \to \infty$ is taken. Although it follows directly from $\lim_{\tau\to 0} p_K(k) = p_0(k)$ that $\lim_{\tau\to 0} \mu_K = \lambda T_{\rm b}$, a direct proof can also be obtained in the following way; the right-hand side of (54) is a double series whose terms can be ordered in an infinite matrix:

$$e^{-\lambda T_{\rm b}} \times \begin{bmatrix} 0 & \frac{(\lambda T_{\rm b})^1}{1!} & \frac{(\lambda T_{\rm b})^2}{2!} & & \frac{(\lambda T_{\rm b})^m}{m!} & \\ 0 & 0 & \frac{(\lambda T_{\rm b})^2}{2!} & \cdots & \frac{(\lambda T_{\rm b})^m}{m!} & \cdots \\ 0 & 0 & 0 & & \frac{(\lambda T_{\rm b})^m}{m!} & \\ & \vdots & & \ddots & \vdots & \\ 0 & 0 & 0 & \cdots & \frac{(\lambda T_{\rm b})^m}{m!} & \cdots \\ & \vdots & & & \vdots & \ddots \end{bmatrix} ,$$

The rows and columns of the above matrix are indexed by summation indices of (54), k and i, respectively. Summation of the first m rows of this matrix gives:

$$\begin{aligned} S_m &= e^{-\lambda T_\mathrm{b}} \times \left[\sum_{i=0}^{m} i \times \frac{(\lambda T_\mathrm{b})^i}{i!} + m \times \sum_{i=m+1}^{\infty} \frac{(\lambda T_\mathrm{b})^i}{i!} \right] \\ &= e^{-\lambda T_\mathrm{b}} \times \left[(\lambda T_\mathrm{b}) \times \sum_{i=0}^{m-1} \frac{(\lambda T_\mathrm{b})^i}{i!} \right. \\ &\qquad \left. + m \times \sum_{i=0}^{\infty} \frac{(\lambda T_\mathrm{b})^i}{i!} - m \times \sum_{i=0}^{m} \frac{(\lambda T_\mathrm{b})^i}{i!} \right], \end{aligned} \tag{55}$$

As m goes to infinity, the summation of the second and third terms clearly goes to zero. Furthermore, using the Taylor series expression $\lim_{m\to\infty} \sum_{i=0}^{m-1} (\lambda T_\mathrm{b})^i/i! = e^{\lambda T_\mathrm{b}}$, one has:

$$\lim_{\tau\to 0} \mu_K = \lim_{m\to\infty} S_m = \lambda T_\mathrm{b} \,. \tag{56}$$

With an approach similar to the one used for deriving μ_K, the variance of the distribution in (27) can be obtained as:

$$\begin{aligned} \sigma_K^2 = & \sum_{k=0}^{k_\mathrm{max}-2} \sum_{i=0}^{k} (2k_\mathrm{max} - 2k - 3) \psi(i, \lambda_{k+1}) \\ & - \left(\sum_{k=0}^{k_\mathrm{max}-2} \sum_{i=0}^{k} \psi(i, \lambda_{k+1}) \right)^2 . \end{aligned} \tag{57}$$

and the limiting relation $\lim_{\tau\to 0} \sigma_K^2 = \lambda T_\mathrm{b}$ is verified, where the product λT_b is the variance of the original Poisson distribution.

Appendix C
Mean and Variance of the PQ PMF

According to (5) and (36), the generating function $G(z,t)$ and its derivatives are given by:

$$\begin{aligned} G(z, T_\mathrm{b}) &= \sum_{k=0}^{k_\mathrm{max}-1} p_K(k) z^k \\ &= \sum_{i=0}^{k_\mathrm{max}-1} (z-1)^i \frac{\lambda^i e^{-i\lambda\tau}}{i!} (T_\mathrm{b} - i\tau)^i, \end{aligned} \tag{58}$$

$$\begin{aligned} \frac{\partial G(z, T_\mathrm{b})}{\partial z} &= \sum_{k=0}^{k_\mathrm{max}-1} k p_K(k) z^{k-1} \\ &= \sum_{i=1}^{k_\mathrm{max}-1} i(z-1)^{i-1} \frac{\lambda^i e^{-i\lambda\tau}}{i!} (T_\mathrm{b} - i\tau)^i, \end{aligned} \tag{59}$$

$$\begin{aligned} \frac{\partial^2 G(z, T_\mathrm{b})}{\partial z^2} &= \sum_{k=0}^{k_\mathrm{max}-1} k(k-1) p_K(k) z^{k-2} \\ &= \sum_{i=2}^{k_\mathrm{max}-1} i(i-1)(z-1)^{i-2} \frac{\lambda^i e^{-i\lambda\tau}}{i!} (T_\mathrm{b} - i\tau)^i. \end{aligned} \tag{60}$$

Therefore, the mean and variance of the distribution function in (36) are derived as:

$$\mu_K = \sum_{k=0}^{k_\mathrm{max}} k p_K(k) = \left. \frac{\partial G(z, T_\mathrm{b})}{\partial z} \right|_{z=1} = \lambda e^{-\lambda\tau} (T_\mathrm{b} - \tau). \tag{61}$$

$$\begin{aligned} \sigma_K^2 &= \sum_{k=0}^{k_\mathrm{max}} k^2 p_K(k) - \left(\sum_{k=0}^{k_\mathrm{max}} k p_K(k) \right)^2 \\ &= \left[\frac{\partial^2 G(z, T_\mathrm{b})}{\partial z^2} + \frac{\partial G(z, T_\mathrm{b})}{\partial z} - \left(\frac{\partial G(z, T_\mathrm{b})}{\partial z} \right)^2 \right] \Bigg|_{z=1} \\ &= \lambda^2 e^{-2\lambda\tau} (3\tau^2 - 2T_\mathrm{b}\tau) + \lambda e^{-\lambda\tau} (T_\mathrm{b} - \tau). \end{aligned} \tag{62}$$

Finally, the limiting expressions $\lim_{\tau\to 0} \mu_K = \lambda T_\mathrm{b}$ and $\lim_{\tau\to 0} \sigma_K^2 = \lambda T_\mathrm{b}$ are verified.

Appendix D
Threshold detection for AQ SPADs with $\lambda_\mathrm{n} \gg 1$ or $\tau \ll T_\mathrm{b}$

With the approximate PMF given in (51), the likelihood ratio test in (44) reduces to:

$$L(k) = \frac{\psi(k, \lambda_{k+1}^{\mathrm{sn}})}{\psi(k, \lambda_{k+1}^{\mathrm{n}})} \underset{H_0}{\overset{H_1}{\gtrless}} 1 \tag{63}$$

where $\lambda_{k+1}^{\mathrm{n}} = \lambda_\mathrm{n}(T_\mathrm{b} - (k+1)\tau)$ and $\lambda_{k+1}^{\mathrm{sn}} = (\lambda_\mathrm{s} + \lambda_\mathrm{n})(T_\mathrm{b} - (k+1)\tau)$. Substituting $\psi(i,\lambda) = \lambda^i e^{-\lambda}/i!$ gives:

$$L(k) = e^{-\lambda_\mathrm{s}(T_\mathrm{b} - (k+1)\tau)} \left(\frac{\lambda_\mathrm{s} + \lambda_\mathrm{n}}{\lambda_\mathrm{n}} \right)^k \underset{H_0}{\overset{H_1}{\gtrless}} 1 \tag{64}$$

Finally, taking the natural logarithm from both sides gives:

$$k \underset{H_0}{\overset{H_1}{\gtrless}} \frac{\lambda_\mathrm{s} T_\mathrm{b} - \lambda_\mathrm{s}\tau}{\lambda_\mathrm{s}\tau + \ln\left(1 + \frac{\lambda_\mathrm{s}}{\lambda_\mathrm{n}}\right)} \,. \tag{65}$$

Therefore, for an AQ SPAD, the maximum likelihood detection simplifies to a threshold detection if $\lambda_\mathrm{n} \gg 1$ or $\tau \ll T_\mathrm{b}$.

Appendix E
Special Property of an AQ SPAD in Threshold Detection

Here, the error probability of threshold detection for an AQ SPAD is derived. Assuming $m_\mathrm{T} < T/\tau$, the probability of counting at most m_T photons, is calculated as:

$$\begin{aligned} \sum_{k=0}^{m_\mathrm{T}} p_K(k) &\overset{(*)}{=} \sum_{i=0}^{m_\mathrm{T}} \sum_{k=i}^{m_\mathrm{T}} \psi(i, \lambda_{k+1}) - \sum_{i=0}^{m_\mathrm{T}-1} \sum_{k=i+1}^{m_\mathrm{T}} \psi(i, \lambda_k) \\ &\overset{(**)}{=} \psi(m_\mathrm{T}, \lambda_{m_\mathrm{T}+1}) \\ &\quad + \sum_{i=0}^{m_\mathrm{T}-1} \left[\sum_{k=i}^{m_\mathrm{T}} \psi(i, \lambda_{k+1}) - \sum_{k'=i}^{m_\mathrm{T}-1} \psi(i, \lambda_{k'+1}) \right] \\ &= \psi(m_\mathrm{T}, \lambda_{m_\mathrm{T}+1}) + \sum_{i=0}^{m_\mathrm{T}-1} \psi(i, \lambda_{m_\mathrm{T}+1}) \\ &= \sum_{i=0}^{m_\mathrm{T}} \psi(i, \lambda_{m_\mathrm{T}+1}) \end{aligned} \tag{66}$$

where, in $(*)$, the order of summations is changed and for $(**)$, a change of variable $k' = k-1$ is used. According to (66), the probability of counting up to m_T photons, for an AQ SPAD receiver with dead time τ in a bit interval of T_b seconds, is the same as that of a SPAD receiver without

dead time counting photons at the same rate, but during a bit interval of $T_{\rm b} - (m_{\rm T}+1)\tau$ seconds, or the same as that of a similar SPAD without dead time, but with a quantum efficiency reduced by the factor $(1-(m_{\rm T}+1)\tau/T_{\rm b})$. This result greatly simplifies the error probability calculations for an AQ SPAD.

ACKNOWLEDGMENT

Professor Harald Haas acknowledges support by the UK Engineering and Physical Sciences Research Council (EPSRC) under Grant EP/K008757/1.

REFERENCES

[1] R. M. Gagliardi and S. Karp, *Optical Communications*, 2nd ed. New York: Wiley, 1995.

[2] S. B. Alexander, *Optical Communication Receiver Design*. Bellingham: SPIE Press, 1997.

[3] R. H. Hadfield, "Single-Photon Detectors for Optical Quantum Information Applications," *Nat. Photon.*, vol. 3, no. 12, pp. 696–705, Nov. 2009.

[4] C. Niclass *et al.*, "Design and Characterization of a CMOS 3-D Image Sensor Based on Single Photon Avalanche Diodes," *IEEE J. Solid-State Circuits*, vol. 40, no. 9, pp. 1847–1854, Sep. 2005.

[5] A. Tosi, F. Zappa, and S. Cova, "Single-Photon Detectors for Practical Quantum Cryptography," in *Proc. SPIE, Electr.-Opt. Remote Sensing, Photonic Technol. Appl. VI*, vol. 8542, Edinburgh, UK, 2012, p. 8.

[6] Y. Li *et al.*, "Single Photon Avalanche Diode (SPAD) VLC System and Application to Downhole Monitoring," in *Proc. IEEE Global Commun. Conf.*, Austin, TX, 2014, pp. 2108–2113.

[7] Y. Li, M. Safari, R. Henderson, and H. Haas, "Optical OFDM with Single-Photon Avalanche Diode," *IEEE Photon. Technol. Lett.*, vol. 27, no. 9, pp. 943–946, May 2015.

[8] ——, "Nonlinear Distortion in SPAD-Based Optical OFDM Systems," in *Proc. IEEE Global Commun. Conf. Workshops*, San Diego, CA, 2015.

[9] O. Almer, D. Tsonev *et al.*, "A SPAD-Based Visible Light Communications Receiver Emng Higher Order Modulation," in *Proc. IEEE Global Communications Conf.*, San Diego, CA, 2015.

[10] J. Kosman, O. Almer, A. V. Jalajakumari, S. Videv, H. Haas, and R. K. Henderson, "60 Mb/s, 2 Meters Visible Light Communications in 1 klx Ambient Using an Unlensed CMOS SPAD Receiver," in *Photonics Society Summer Topical Meeting Series*, Newport Beach, CA, 2016, pp. 171–172.

[11] M. A. Khalighi, T. Hamza *et al.*, "Underwater Wireless Optical Communications Using Silicon Photo-Multipliers," *IEEE Photonics J.*, vol. 9, no. 4, pp. 1–10, Aug. 2017.

[12] C. Wang, H.-Y. Yu, and Y.-J. Zhu, "A Long Distance Underwater Visible Light Communication System with Single Photon Avalanche Diode," *IEEE Photonics Journal*, vol. 8, no. 5, pp. 1–11, 2016.

[13] A. Spinelli and A. Lacaita, "Physics and Numerical Simulation of Single Photon Avalanche Diodes," *IEEE Trans. Electron Devices*, vol. 44, no. 11, pp. 1931–1943, Nov. 1997.

[14] M. W. Fishburn, "Fundamentals of CMOS Single-Photon Avalanche Diodes," Ph.D. dissertation, Dept. Elect. Eng., TU Delft, Delft, Netherlands, 2012.

[15] A. Migdall, S. V. Polyakov, J. Fan, and J. C. Bienfang, *Single-Photon Generation and Detection: Physics and Applications*. Academic Press, Nov. 2013, vol. 45.

[16] A. Gallivanoni, I. Rech, and M. Ghioni, "Progress in Quenching Circuits for Single Photon Avalanche Diodes," *IEEE Trans. Nucl. Sci.*, vol. 57, no. 6, pp. 3815–3826, Dec. 2010.

[17] D. Chitnis and S. Collins, "A SPAD-Based Photon Detecting System for Optical Communications," *J. Lightw. Technol.*, vol. 32, no. 10, pp. 2028–2034, May 2014.

[18] D. Chitnis, L. Zhang *et al.*, "A 200 Mb/s VLC Demonstration with a SPAD Based Receiver," in *IEEE Summer Topicals Meeting Series*, Jul. 2015, pp. 226–227.

[19] E. Fisher, I. Underwood, and R. Henderson, "A Reconfigurable 14-bit 60GPhoton/s Single-Photon Receiver for Visible Light Communications," in *Proc. European Solid-State Circuits Conf.*, Bordeaux, France, 2012, pp. 85–88.

[20] ——, "A Reconfigurable Single-Photon-Counting Integrating Receiver for Optical Communications," *IEEE J. Solid-State Circuits*, vol. 48, no. 7, pp. 1638–1650, Jul. 2013.

[21] J. H. Lee, I. J. Kim, and H. D. Choi, "On the Dead Time Problem of a GM Counter," *Appl. Radiat. Isot.*, vol. 67, no. 6, pp. 1094–1098, Jun. 2009.

[22] A. Eisele *et al.*, "185 MHz Count Rate, 139 dB Dynamic Range Single-Photon Avalanche Diode with Active Quenching Circuit in 130 nm CMOS Technology," in *Proc. Int. Image Sensor Workshop*, Japan, 2011, pp. 278–281.

[23] K. Omote, "Dead-Time Effects in Photon Counting Distributions," *Nuclear Instruments and Methods in Physics Research Section A: Accelerators, Spectrometers, Detectors and Associated Equipment*, vol. 293, no. 3, pp. 582–588, Aug. 1990.

[24] C.-C. Chen, "Effect of Detector Dead Time on the Performance of Optical Direct-Detection Communication Links," *TDA Progress Rep.*, vol. 42–93, pp. 146–154, 1988.

[25] D. Zou, C. Gong, K. Wang, and Z. Xu, "Characterization of a Practical Photon Counting Receiver in Optical Scattering Communication," in *Proc. IEEE Global Commun. Conf.*, Singapore, 2017.

[26] E. Sarbazi and H. Haas, "Detection Statistics and Error Performance of SPAD-based Optical Receivers," in *Proc. IEEE 26th Ann. Int. Symp. Personal, Indoor, and Mobile Radio Communications*, Hong Kong, China, 2015, pp. 830–834.

[27] E. Sarbazi, M. Safari, and H. Haas, "Photon Detection Characteristics and Error Performance of SPAD Array Optical Receivers," in *Proc. IEEE 4th Int. Workshop on Optical Wireless Communications*, Istanbul, Turkey, 2015, pp. 132–136.

[28] ——, "On the Information Transfer Rate of SPAD Receivers for Optical Wireless Communications," in *Proc. IEEE Global Communications Conf.*, Washington, DC, Dec. 2016, pp. 1–6.

[29] D. R. Cox, *Renewal Theory*. New York: John Wiley & Sons Inc., 1962.

[30] D. Zwillinger, *Table of Integrals, Series, and Products*, 8th ed. New York: Academic Press, 2014.

[31] D. F. Yu and J. A. Fessler, "Mean and Variance of Single Photon Counting with Deadtime," *Phys. Med. Biol.*, vol. 45, no. 7, pp. 2043–2056, 2000.

Elham Sarbazi (S'15) received her B.Sc. in Electrical and Computer Engineering from the University of Tehran, Tehran, Iran, in 2011, and her M.Sc. (Hons.) in Electrical Engineering with a focus in communication systems from the Ozyegin University, Istanbul, Turkey, in 2014. She is currently working toward her Ph.D. degree in Electrical Engineering, at the Institute for Digital Communications, the University of Edinburgh, Edinburgh, UK. Her main research interests are in optical wireless and visible light communications.

Majid Safari (S'08-M'11) received his Ph.D. degree in Electrical and Computer Engineering from the University of Waterloo, Canada in 2011. He also received his B.Sc. degree in Electrical and Computer Engineering from the University of Tehran, Iran, in 2003, M.Sc. degree in Electrical Engineering from Sharif University of Technology, Iran, in 2005. He is currently an assistant professor in the Institute for Digital Communications at the University of Edinburgh. Before joining Edinburgh in 2013, he held postdoctoral fellowship at McMaster University, Canada. Dr. Safari is currently an associate editor of IEEE Communication letters and was the TPC co-chair of the 4th International Workshop on Optical Wireless Communication in 2015. His main research interest is the application of information theory and signal processing in optical communications including fiber-optic communication, free-space optical communication, visible light communication, and quantum communication.

Harald Haas (S'98-AM'00-M'03-SM'17) received the Ph.D. degree from the University of Edinburgh in 2001. He currently holds the Chair of Mobile Communications at the University of Edinburgh, and is the Initiator, Co-Founder, and the Chief Scientific Officer of pureLiFi Ltd., and the Director of the LiFi Research and Development Center, the University of Edinburgh. He has authored 400 conference and journal papers, including a paper in Science and co-authored the book *Principles of LED Light Communications Towards Networked Li-Fi* (Cambridge University Press, 2015). His main research interests are in optical wireless communications, hybrid optical wireless and RF communications, spatial modulation, and interference coordination in wireless networks. He first introduced and coined spatial modulation and LiFi. LiFi was listed among the 50 best inventions in *TIME* Magazine 2011. He was an invited speaker at TED Global 2011, and his talk on "Wireless Data from Every Light Bulb" has been watched online over 2.4 million times. He gave a second TED Global lecture in 2015 on the use of solar cells as LiFi data detectors and energy harvesters. This has been viewed online over 1.8 million times. He was elected as a fellow of the Royal Society of Edinburgh in 2017. In 2012 and 2017, he was a recipient of the prestigious Established Career Fellowship from the Engineering and Physical Sciences Research Council (EPSRC) within Information and Communications Technology in the U.K. In 2014, he was selected by EPSRC as one of ten Recognising Inspirational Scientists and Engineers (RISE) Leaders in the U.K. He was a co-recipient of the EURASIP Best Paper Award for the *Journal on Wireless Communications and Networking* in 2015, and co-recipient of the Jack Neubauer Memorial Award of the IEEE Vehicular Technology Society. In 2016, he received the Outstanding Achievement Award from the International Solid State Lighting Alliance. He was a co-recipient of recent best paper awards at VTC-Fall, 2013, VTC-Spring 2015, ICC 2016, and ICC 2017. He is an Editor of the IEEE TRANSACTIONS ON COMMUNICATIONS and the IEEE JOURNAL OF LIGHTWAVE TECHNOLOGIES.